analytical chemistry

pubs.acs.org/ac Article

3D Matrix-Arranged AuAg Nanoclusters As Electrochemiluminescence Emitters for Click Chemistry-Driven Signal Switch Bioanalysis

Fang Yang, Xin-Ya Jiang, Wen-Bin Liang, Ya-Qin Chai, Ruo Yuan, and Ying Zhuo*

Cite This: *Anal. Chem.* 2020, 92, 2566−2572 Read Online

ACCESS | Metrics & More | Article Recommendations | Supporting Information

ABSTRACT: We hereby described an electrochemiluminescence (ECL) biosensor for glutathione (GSH) based on a 3D DNA matrix with ordered binding sites and cavity structure that self-assembled from tetrahedral DNA blocks (TDBs). First, the alkyne-labeled TDBs were employed to build an alkyne-rich 3D matrix (C≡C-3DM) on the electrode surface. Then, the GSH-induced click chemistry was triggered as a signal switch to introduce the large amounts of N_3-DNA decorated AuAg nanoclusters (N_3−AuAg NCs) into C≡C-3DM for signal output. In particular, the presence of GSH could induce the formation of GSH−Cu(I) complex by the redox reaction between GSH and Cu(II), which could act as an initiator to link the N_3−AuAg NCs with C≡C-3DM according to the Huisgen 1,3-dipolar cycloaddition reaction. By this way, numerous N_3−AuAg NCs were orderly bonded to the 3D matrix to effectively reduce their agglomeration and inner filter effect, achieving a remarkable ECL enhancement. As a result, the proposed GSH biosensor showed a wide linear range from 5 to 200 μM with a low detection limit of 0.90 μM. In general, this work provided a rapid, highly efficient, and convenient signal amplification for small-molecule detection and broadened the application of TDBs in biosensing.

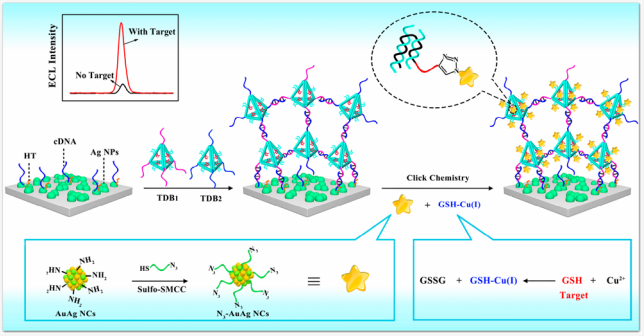

As a class of fascinating nanomaterials, bimetallic nanoclusters (NCs) with excellent optical and electronic properties have found great applications in many areas, such as biology, sensing, and catalysis.[1−3] However, to disperse the NCs in solution or directly confine them on the sensing interface would unavoidably produce high excess luminophore or inner filter effect, obstructing their further application.[4,5] As an emerging field, DNA nanotechnology presented unique advantages in creating nanoscale structures and devices with controlled sizes and shapes.[6] Among the diverse nanostructures created by DNA nanotechnology, the tetrahedral DNA block (TDB) structure has proven to be an excellent candidate for loading biomolecules, benefiting from its mechanical rigidity, structural stability, ordered binding sites, and easy multiple-modification properties.[7−9] For instance, Fan's group designed a multivalent TDB for intracellular delivery of immunostimulatory CpG oligonucleotides.[10] Medintz and colleagues used a peptide-modified TDB as a nanocage for carrying quantum dots (QDs).[11] Inspired by these, the alkyne-rich 3D matrix (C≡C-3DM) self-assembled from two alkyne-labeled tetrahedral DNA blocks (TDB_1 and TDB_2) was first proposed to orderly arrange the N_3-DNA decorated AuAg NCs (N_3−AuAg NCs), which combined the programmability of the DNA structure and the high efficiency of click chemistry. More importantly, to the best of our knowledge, this is also the first attempt to minimize the inner filter effect of AuAg NCs emitters using the C≡C-3DM with cavity structure and ordered recognition sites.

Glutathione (GSH, L-γ-glutamyl-L-cysteinyl-glycine) is a non-nucleic acid tripeptide that plays a crucial role in maintaining the redox activities of biological systems.[12,13] However, the overexpression of GSH would break the redox balance, leading to many diseases such as cancer, aging, and other ailments.[14,15] Thus, the development of a rapid, reliable, and sensitive method for GSH is particularly important. Recently, target conversion strategies have provided an excellent opportunity for highly sensitive detection of the non-nucleic acid target, where the non-nucleic acid target could combine with its aptamer to form the target−aptamer complex and further initiate nucleic acid recycling to output numerous substitute targets for signal amplification.[16−18] However, the aptamers selected for recognizing GSH have not been reported so far, making it difficult to detect the trace GSH by nucleic acid amplification. Herein, a novel GSH

Received: September 18, 2019
Accepted: January 10, 2020
Published: January 10, 2020

https://dx.doi.org/10.1021/acs.analchem.9b04256
Anal. Chem. 2020, 92, 2566−2572

Scheme 1. Preparation of the TDB_1 and TDB_2 (A); Working Principle of the Biosensor for GSH Detection (B)

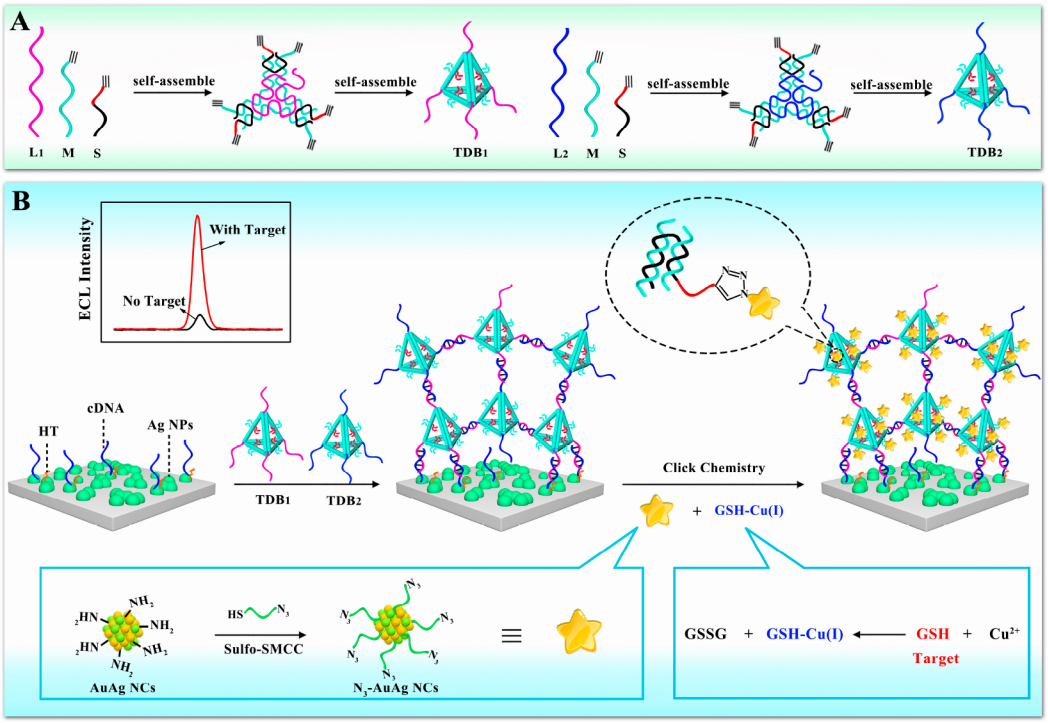

conversion strategy was developed based on the redox reaction between GSH and Cu(II) to convert GSH into GSH−Cu(I) complex, which could act as a catalyst for the Huisgen 1,3-dipolar cycloaddition reaction, allowing the attachment of N_3−AuAg NCs to C≡C-3DM to generate an ECL signal. This conversion strategy provided a new direction for developing more rapid, efficient, and convenient GSH biosensors because (i) GSH could react rapidly with Cu(II) and subsequently form a stable GSH−Cu(I) complex within 0.2 s;[19] (ii) the GSH−Cu(I) complex has high selectivity toward click chemistry;[20] and (iii) it eliminated the need for complicated/tedious synthesis and purification procedures.

Herein, an ultrasensitive GSH biosensor was constructed by using GSH-induced click chemistry as a signal switch and 3D matrix-arranged AuAg NCs as ECL emitters. As depicted in Scheme 1, the Ag nanoparticles (NPs) obtained by a polyol process could not only be used to immobilize capture DNA (cDNA) but also be used as a coreaction accelerator to construct a ternary AuAg NCs/triethylamine (TEA)/Ag NPs system for ECL signal amplification. Hereafter, TDB_1 was captured by cDNA and further hybridized with TDB_2 to form C≡C-3DM on the electrode surface. With the addition of target GSH, the GSH−Cu(I) complex was formed by the redox reaction between GSH and Cu(II), which subsequently acted as a catalyst of click chemistry to facilitate the connection between the N_3−AuAg NCs and C≡C-3DM, achieving the signal output. It is worth noting that this work not only demonstrated that the 3D matrix could serve as an efficient platform for arranging AuAg NCs with enhanced ECL performance but also opened up the potentiality for developing simple, economical, and sensitive ECL biosensors for bioanalysis and diagnosis.

EXPERIMENTAL SECTION

Preparation and Decoration of AuAg Nanoclusters. The preparation of the AuAg nanoclusters (NCs) was based on a protocol by Hikosou et al. with slight modification.[21] In total, 0.5 mL of $HAuCl_4$ (20 mM) and 0.1 mL of $AgNO_3$ (20 mM) were added into a 25 mL round-bottom flask with 4.35 mL of deionized water. Subsequently, 0.15 mL of GSH (100 mM) was added to the flask, and the resulting mixture was stirred at 25 °C for 5 min. After refluxing for 24 h at 70 °C, the synthesized AuAg NCs were purified with filter membranes (MWCO 3K) under ultracentrifugation (15 000 rpm, 15 min) and then stored in the dark at 4 °C.

The purified AuAg NCs were subsequently decorated with N_3-DNA. Briefly, the N_3-DNA containing thiol moieties reacted with tris(2-carboxyethyl)phosphine (TCEP) (1.0 mM) for 1 h to reduce the disulfide bonds. Concurrently, the purified AuAg NCs were dissolved in phosphate-buffered saline (PBS) (0.1 M, pH 7.4) at a concentration of 10 μg mL^{-1}, and then 2.4 mg of Sulfo-SMCC cross-linker was introduced to activate the AuAg NCs for 1 h at room temperature. Then, the activated AuAg NCs were collected after the removal of excess cross-linkers. Thereafter, the N_3-DNA reacted with the activated AuAg NCs for 3 h at room temperature. Following the reaction, the N_3-DNA decorated AuAg NCs (N_3−AuAg NCs) were purified with filter membranes (MWCO 3K) under ultracentrifugation (15 000 rpm, 15 min). Finally, the purified N_3−AuAg NCs were stored at 4 °C until use.

Assembly of the Tetrahedral DNA Blocks. Tetrahedral DNA blocks (TDB_1 and TDB_2) were formed by the self-assembly of L_1, M, and S and L_2, M, and S, respectively. In total, L_1, M, and S and L_2, M, and S at a designated molar ratio (1:3:3) were mixed in Tris-acetic-EDTA-Mg^{2+} (TAE/Mg^{2+}) buffer, respectively. The DNA solution was then annealed at 95

https://dx.doi.org/10.1021/acs.analchem.9b04256
Anal. Chem. 2020, 92, 2566−2572

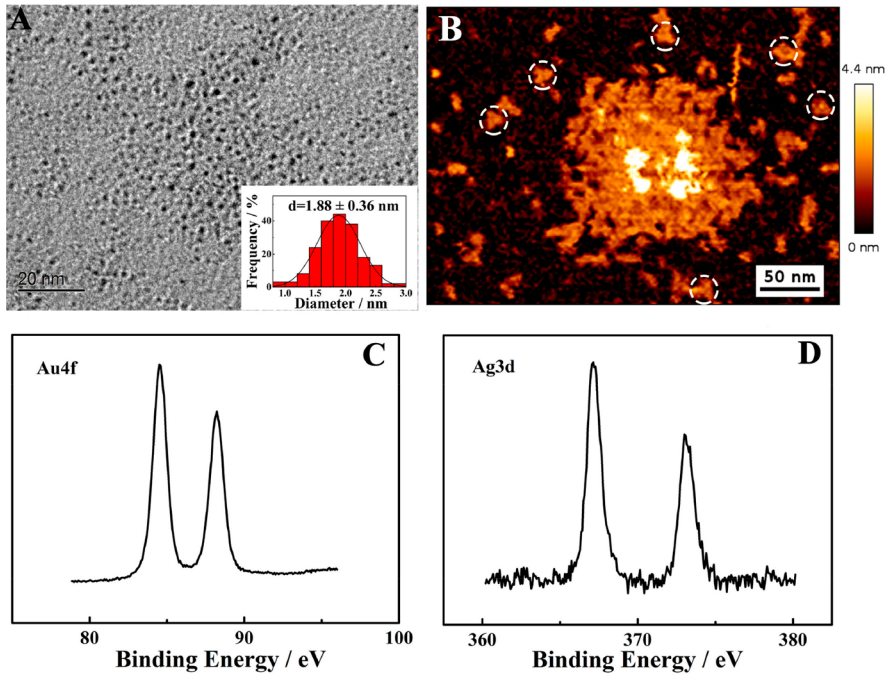

Figure 1. TEM image and size distribution of the prepared AuAg NCs (A). AFM image of C≡C-3DM (B), and XPS spectra of Au 4f region (C) and Ag 3d region (D).

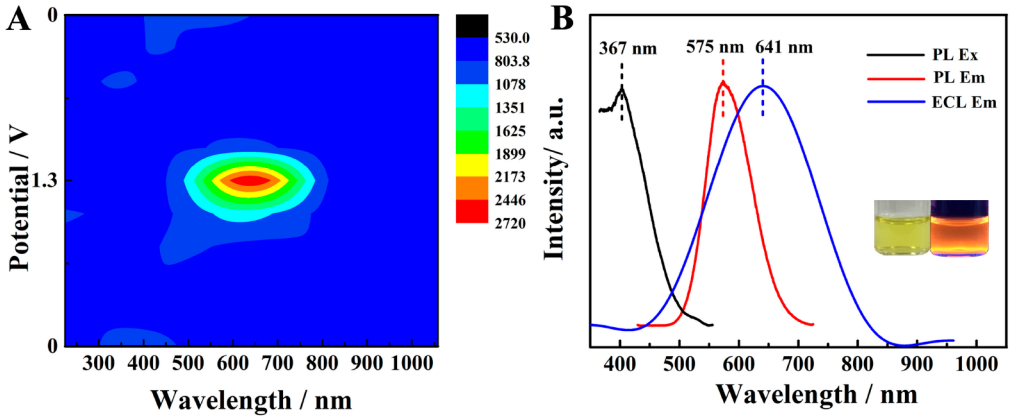

Figure 2. Heat map image of the prepared AuAg NCs (A). PL excitation (PL Ex), PL emission (PL Em) spectrum, and maximum ECL emission (ECL Em) of the AuAg NCs (B). Insets in B are the images of AuAg NCs under visible light and UV light irradiation (λex = 365 nm).

°C for 10 min, followed by being slowly cooled down to room temperature over 48 h.

Fabrication of the GSH Biosensor. The pretreatment of the bare glassy carbon electrode (GCE) was first performed using our previous method.[22] After that, 10 μL of Ag NPs was dropped onto the pretreated GCE and evaporated at room temperature. Then, 5 μL of cDNA (2.0 μM) was decorated on the Ag NPs/GCE by incubation for 12 h at 4 °C. After rinsing with deionized water, 10 μL of Hexanethiol (HT) (1 mM) was incubated on the cDNA/Ag NPs/GCE for 1 h to minimize the nonspecific adsorption. Subsequently, 5 μL of TDB_1 and 5 μL of TDB_2 were dropped onto the HT/cDNA/Ag NPs/GCE for further hybridization at 37 °C for 2.5 h to form the alkyne-rich 3D matrix (C≡C-3DM). Finally, 15 μL of N_3−AuAg NCs and 5 μL of solution containing 200 μM Cu^{2+} and different concentrations of GSH were pipetted onto C≡C-3DM/HT/cDNA/Ag NPs/GCE, followed by reaction for 1.5 h at room temperature.

RESULTS AND DISCUSSION

Characterization of the AuAg NCs and C≡C-3DM. The morphology of AuAg NCs was inspected by high-resolution transmission electron microscopy (HRTEM). As shown in Figure 1A, the synthesized AuAg NCs were monodispersed and had an average diameter of 1.88 ± 0.36 nm as judged from statistical evaluation of 195 individual particles in the TEM image (inset in Figure 1A). X-ray photoelectron spectroscopy (XPS) was further used to explore the valence state of Au and Ag in the AuAg NCs. From the Au XPS spectrum (Figure 1C), the binding energies at 88.2 and 84.5 eV stood for Au $4f_{5/2}$ and Au $4f_{7/2}$, respectively. Note that the binding energy of $4f_{7/2}$ fell between the Au(0) binding energy of bulk Au metal (84.0 eV) and the Au(I) binding energy (86 eV) of gold thiolate, revealing the presence of Au(0) and Au(I) in the AuAg NCs.[23] The XPS spectrum of Ag is shown in Figure 1D; the binding energies of Ag $3d_{5/2}$ and Ag $3d_{3/2}$ were found at 367.1 and 373.0 eV, respectively, which are

https://dx.doi.org/10.1021/acs.analchem.9b04256
Anal. Chem. 2020, 92, 2566−2572

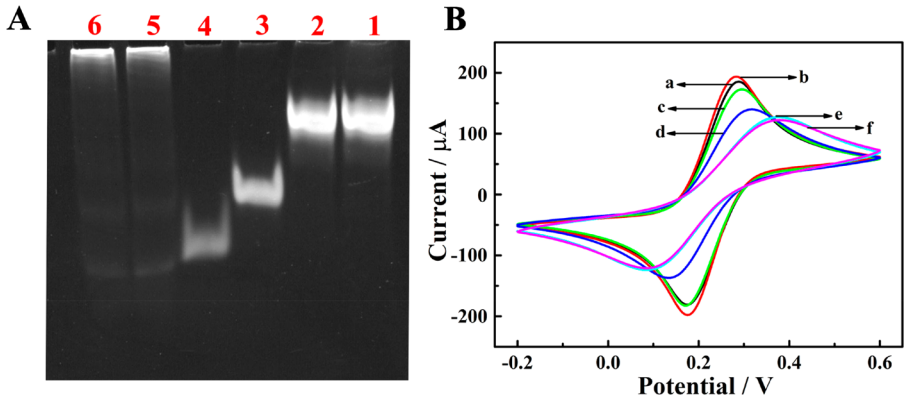

Figure 3. PAGE analysis of the self-assembled TDBs: lane 1, L_1; lane 2, L_2; lane 3, M; lane 4, S; lane 5, TDB_1; lane 6, TDB_2 (A). CV curves of (a) bare GCE, (b) Ag NPs/GCE, (c) cDNA/Ag NPs/GCE, (d) HT/cDNA/Ag NPs/GCE, (e) C≡C-3DM/HT/cDNA/Ag NPs/GCE, and (f) N_3−AuAg NCs/C≡C-3DM/HT/cDNA/Ag NPs/GCE (B).

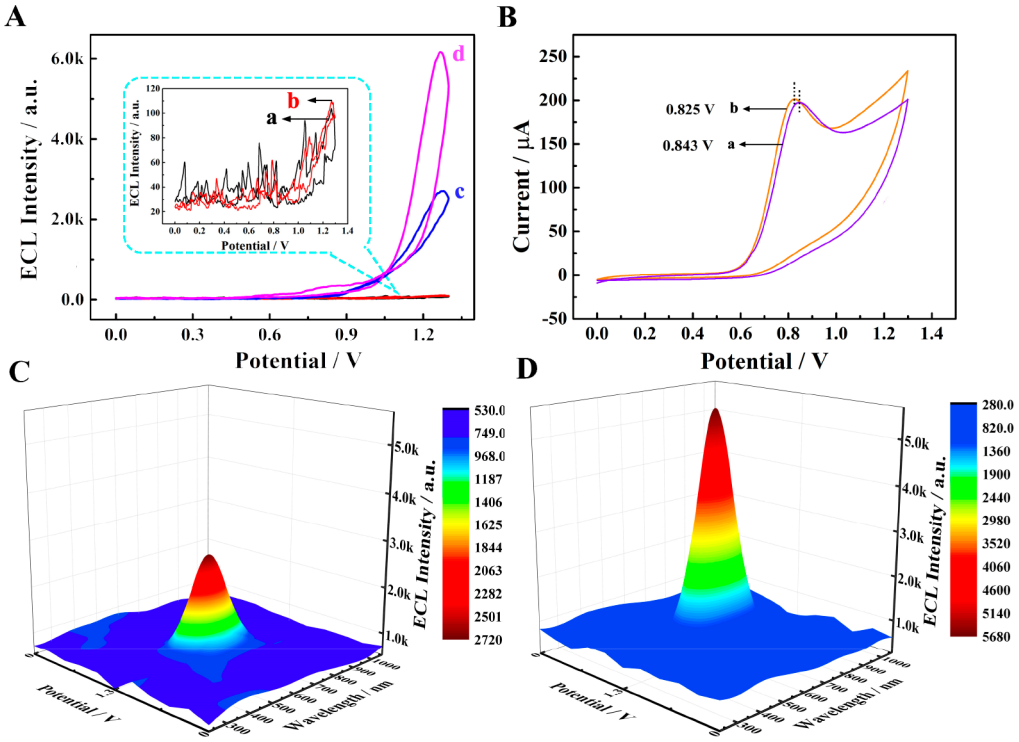

Figure 4. ECL response of bare GCE (a) and Ag NPs/GCE (b) in PBS containing AuAg NCs and of bare GCE (c) and Ag NPs/GCE (d) in PBS containing AuAg NCs and coreactant TEA (A). CV curves of bare GCE (a) and Ag NPs/GCE (b) in PBS containing TEA (B). 3D ECL spectrum of bare GCE (C) and Ag NPs/GCE (D) in PBS containing AuAg NCs and coreactant TEA.

identical to those of the Ag(I) species.[24] (The full XPS spectrum of AuAg NCs and XPS analysis of Ag NPs are listed in the Supporting Information, Figure S3.) The atomic force microscopy (AFM) imaging was applied to visualize the C≡C-3DM. As shown in Figure 1B, some free TDBs presented the triangle shapes, which is consistent with previous reports,[25] indicating that the TDBs were synthesized successfully. Meanwhile, large aggregates could be observed, illustrating that the 3D matrix was formed by the hybridization of TDBs.

Spectral Characteristics of the AuAg NCs. The spooling ECL spectroscopy was applied to study the ECL characteristic of the AuAg NCs. As shown in Figure 2A, a heat map image showed that the maximum ECL emission of the prepared AuAg NCs (with coreactant TEA) was located at 641 nm. Compared with the photoluminescence (PL) emission wavelength of AuAg NCs (575 nm, Figure 2B), the ECL spectrum of AuAg NCs was red-shifted about 66 nm, which was similar to the optical phenomenon of previously reported metal NCs, demonstrating that the ECL performance of AuAg NCs was mainly dependent on the surface state.[14,26,27] In addition, the inset in Figure 2B showed that the AuAg NCs dispersion was light yellow under ambient daylight, while it turned to orange with the irradiation of the UV lamp (λ = 365 nm).

Feasibility Investigation. The native polyacrylamide gel electrophoresis (PAGE, 16%) was used to verify the construction of tetrahedral DNA blocks. As displayed in Figure 3A, the L_1, L_2, M, and S in lanes 1, 2, 3, and 4 presented different single bands, respectively. After the one-pot assembly of tetrahedron DNA blocks (TDB_1 and TDB_2) by annealing the mixture of L_1, M, and S ($n_{L1}/n_M/n_S$ = 1:3:3) and L_2, M,

https://dx.doi.org/10.1021/acs.analchem.9b04256
Anal. Chem. 2020, 92, 2566−2572

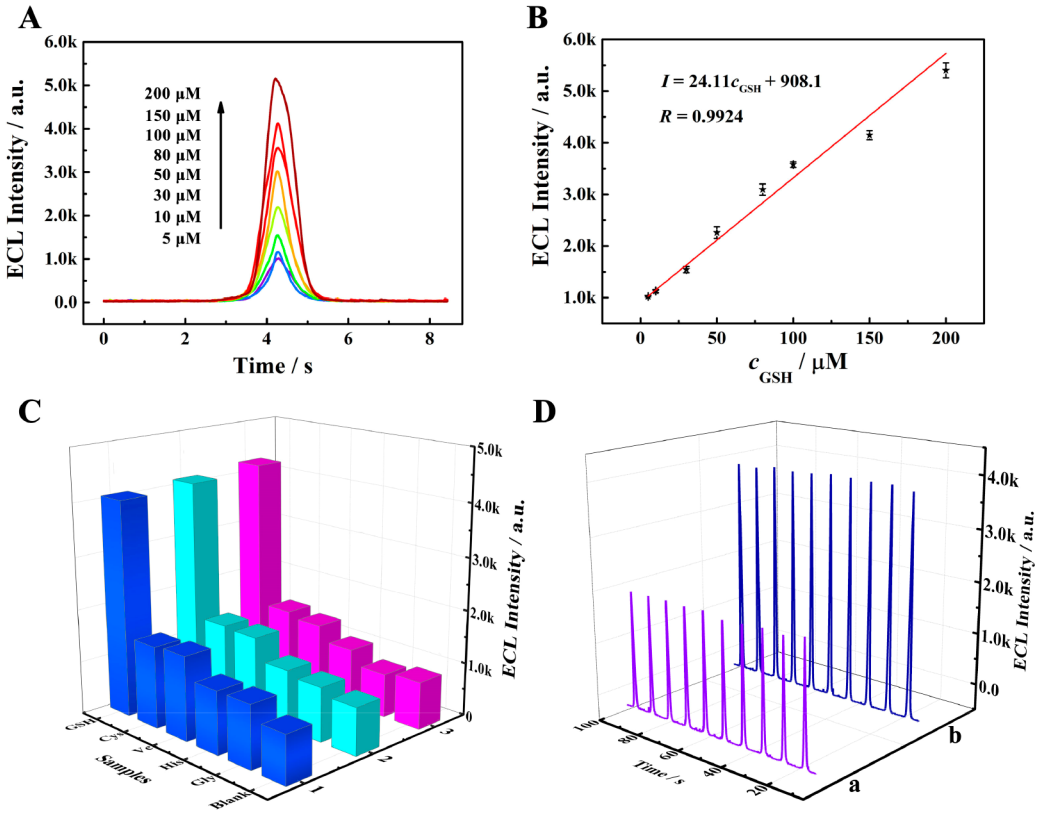

Figure 5. ECL response toward different concentrations of GSH (A). Linear calibration curve for GSH detection (B). Selectivity of the ECL biosensor for GSH detection toward different interfering substances (C). The concentration of Gly and His was 1 mM; the concentration of Vc and Cys was 20 μM. Stability of the biosensor (D). The concentrations of GSH were 50 μM (a) and 150 μM (b), respectively.

and S ($n_{L2}/n_M/n_S$ = 1:3:3), respectively, two bright bands (lanes 5 and 6) could be clearly observed. It can be seen that the TDB_1 and TDB_2 presented much slower migration than that of L_1, L_2, M, and S, indicating that the successful assembly of TDB_1 and TDB_2.

The cyclic voltammetry (CV) was applied to confirm the step-by-step fabrication of the sensor platform. As shown in Figure 3B, the bare GCE showed a pair of reversible redox peaks of $[Fe(CN)_6]^{3-/4-}$ (curve a). After the bare GCE was covered by Ag NPs, the peak currents increased obviously (curve b), showing the excellent electron conduction of the Ag NPs. When the Ag NPs/GCE was decorated with cDNA, the peak currents decreased (curve c) because the formed DNA monolayer impeded the transmission of the electron. The peak currents were further decreased after incubation with non-conductive molecular HT (curve d). When TDB_1 and TDB_2 were introduced to the modified electrode, the peak currents decreased significantly (curve e), suggesting that a C≡C-3DM was formed by the hybridization of TDB_1 and TDB_2. Finally, the peak currents (curve f) decreased continuously as the N_3−AuAg NCs with negative charges hindered the electron transfer.

Possible Reaction Mechanism of AuAg NCs/TEA/Ag NPs. The possible reaction mechanism was explored by the combination of ECL and CV measurements. As shown in Figure 4A, the ECL intensities of bare GCE (curve a) and Ag NPs/GCE (curve b) had no remarkable difference in PBS containing AuAg NCs (without coreactent TEA), suggesting that Ag NPs had no direct effect on AuAg NCs. Meanwhile, the ECL intensity was noticeably raised to 2700 au when measured in PBS containing AuAg NCs (with coreactant TEA, curve c), illustrating that TEA could act as a coreactant to enhance the ECL emission of AuAg NCs. After the introduction of Ag NPs, the highest ECL emission of 6159 au could be observed (curve d). Meanwhile, the oxidation peak of TEA shifted positively from 0.843 to 0.825 V (Figure 4B), confirming that Ag NPs as the coreaction accelerator could accelerate the oxidation of TEA.

In addition, the 3D ECL spectra was carried out to further confirm that the Ag NPs could act as coreaction accelerator in the AuAg NCs/TEA/Ag NPs system. As shown in Figure 4C, the maximum ECL emission wavelength of AuAg NCs (with coreactant TEA) was 641 nm. When the Ag NPs/GCE was immersed in PBS containing AuAg NCs and coreactant TEA, the maximum ECL emission wavelength had no significant shift (Figure 4D), demonstrating that the luminophore was only AuAg NCs and the Ag NPs could act as a coreaction accelerator in the AuAg NCs/TEA/Ag NPs system.

Finally, the possible mechanism of the AuAg NCs/TEA/Ag NPs ECL system is depicted as follows:

$$TEA - e^- \xrightarrow{Ag\,NPs} TEA^{\cdot +} \quad (1)$$

$$AuAg\,NCs + TEA^{\cdot +} \rightarrow TEA + AuAg\,NCs^{+} \quad (2)$$

$$TEA^{\cdot +} \rightarrow TEA^{\cdot} + H^{+} \quad (3)$$

$$TEA^{\cdot} + AuAg\,NCs \rightarrow Et_2N^{+}CHCH_3 + AuAg\,NCs^{-} \quad (4)$$

$$AuAg\,NCs^{+} + AuAg\,NCs^{-} \rightarrow AuAg\,NCs^{*} \quad (5)$$

$$AuAg\,NCs^{*} \rightarrow AuAg\,NCs + h\nu \quad (6)$$

https://dx.doi.org/10.1021/acs.analchem.9b04256
Anal. Chem. 2020, 92, 2566−2572

ECL Analysis of the Sensing Performance for GSH Detection. Under the optimized conditions, the biosensor was applied to quantitatively determine the GSH with different concentrations. As shown in Figure 5A, the ECL intensities increased gradually with the increasing concentrations of GSH. The relationship between the ECL intensities and the concentration of GSH is presented in Figure 5B. It can be seen that the ECL intensity was proportional to the concentration of GSH in the range from 5 to 200 μM with a detection limit of 0.90 μM. The linear regression equation was $I = 24.11c_{GSH} + 908.1$ with a correlation coefficient of 0.9924. In addition, the performance of the proposed biosensor for the GSH detection was compared with other works (Table 1). The results showed that the biosensor had a comparatively high sensitivity and a low detection limit.

Table 1. Comparison of Other Methods for GSH Detection

methods	detection limit (μM)	linear range (μM)	references
fluorescence	5.3	50−200	28
colorimetric detection	65	0−300	29
electrochemical	100	0.5−7	30
ECL	8.3	24−214	31
ECL	0.90	5−200	this work

To examine the specificity of the biosensor, four different biomolecules, including histidine (His), cysteine (Cys), glycine (Gly), and vitamin C (Vc), were employed as interfering substances. As shown in Figure 5C, the proposed biosensor showed a significant ECL response to the target GSH (150 μM), while the His, Cys, Gly, and Vc showed no notable difference in ECL intensity compared to the blank. Although the Cys and Vc could cause a slight change in ECL, their concentrations (μM levels) were quite lower than the concentration of GSH (mM levels) in biological systems. Therefore, the proposed biosensor could be used for selective GSH detection.

We further investigated the stability of the biosensor by estimating its response to GSH (50 and 150 μM) under 10 continuous cyclic scans. As shown in Figure 5D, the ECL intensities had no obvious fluctuation during continuous scanning, and the relative standard deviations (RSDs) were 1.2% and 0.8%, indicating that the developed biosensor had favorable stability.

Human Serum Sample Measurement. To evaluate the applicability of the developed biosensor, recovery experiments were conducted in human serum. In total, the concentration of GSH in human serum (100-fold diluted) was detected using our method. Subsequently, different concentrations of GSH were spiked into the human serum and detected under the same condition. According to Table 2, the recoveries were in the range 98.5%−101.9%, suggesting that the developed biosensor was feasible for determining GSH in biological systems.

Table 2. Determination of GSH in Human Serum Samples

target	found in sample/μM	added/ μM	total found/μM	recovery/% (n = 3)	RSD/% (n = 3)
GSH	54.72	10	64.57	98.50	6.4
		30	85.30	101.9	6.6
		50	105.1	100.7	5.1

CONCLUSION

In conclusion, an ultrasensitive GSH biosensor was constructed by using 3D matrix-arranged AuAg NCs as ECL emitters and GSH-induced click chemistry as a signal switch. It is worth noting that the C≡C-3DM with abundant binding sites and cavity structures could not only achieve the orderly arrangement of N_3−AuAg NCs but also effectively reduce its agglomeration and inner filter effect, achieving a remarkable ECL enhancement. Furthermore, GSH could react rapidly with Cu(II) and subsequently formed a stable GSH−Cu(I) complex to facilitate the connection between the N_3−AuAg NCs and C≡C-3DM for signal output, which offered a rapid, efficient, and convenient method for non-nucleic acid target detection. Taking these advantages, the proposed biosensor offered a promising alternative means for simple and sensitive detection of GSH.

ASSOCIATED CONTENT

Supporting Information

The Supporting Information is available free of charge at https://pubs.acs.org/doi/10.1021/acs.analchem.9b04256.

Materials and reagents, instrumentation, preparation of Ag NPs, characterization of Ag nanoparticles (NPs), XPS analysis of Ag NPs and full XPS spectrum of AuAg NCs, AFM characterization of TDB_1 and TDB_2, characterization of the fabrication process, optimization of the experimental condition, and relative ECL quantum efficiency of AuAg NCs (PDF)

AUTHOR INFORMATION

Corresponding Author

Ying Zhuo − *Key Laboratory of Luminescent and Real-Time Analytical Chemistry (Southwest University), Ministry of Education, College of Chemistry and Chemical Engineering, Southwest University, Chongqing 400715, P. R. China;* orcid.org/0000-0002-4491-1186; Phone: +86-23-68253172; Email: yingzhuo@swu.edu.cn; Fax: +86-23-68253172

Authors

Fang Yang − *Key Laboratory of Luminescent and Real-Time Analytical Chemistry (Southwest University), Ministry of Education, College of Chemistry and Chemical Engineering, Southwest University, Chongqing 400715, P. R. China*

Xin-Ya Jiang − *Key Laboratory of Luminescent and Real-Time Analytical Chemistry (Southwest University), Ministry of Education, College of Chemistry and Chemical Engineering, Southwest University, Chongqing 400715, P. R. China; Chongqing Key Laboratory of Inorganic Special Functional Materials, College of Chemistry and Chemical Engineering, Yangtze Normal University, Chongqing 408100, P. R. China*

Wen-Bin Liang − *Key Laboratory of Luminescent and Real-Time Analytical Chemistry (Southwest University), Ministry of Education, College of Chemistry and Chemical Engineering, Southwest University, Chongqing 400715, P. R. China;* orcid.org/0000-0002-9086-4974

Ya-Qin Chai − *Key Laboratory of Luminescent and Real-Time Analytical Chemistry (Southwest University), Ministry of Education, College of Chemistry and Chemical Engineering, Southwest University, Chongqing 400715, P. R. China;* orcid.org/0000-0003-4392-9592

https://dx.doi.org/10.1021/acs.analchem.9b04256
Anal. Chem. 2020, 92, 2566−2572

Ruo Yuan − *Key Laboratory of Luminescent and Real-Time Analytical Chemistry (Southwest University), Ministry of Education, College of Chemistry and Chemical Engineering, Southwest University, Chongqing 400715, P. R. China;* orcid.org/0000-0003-3664-6236

Complete contact information is available at: https://pubs.acs.org/10.1021/acs.analchem.9b04256

Notes

The authors declare no competing financial interest.

■ ACKNOWLEDGMENTS

This work was financially supported by the NNSF of China (21675130, 21974108, and 21904013), Natural Science Foundation Project of CQ CSTC (cstc2018jcyjAX0546), and the Fundamental Research Funds for the Central Universities (XDJK2019TJ002), China.

■ REFERENCES

(1) Daniel, M. C.; Astruc, D. *Chem. Rev.* **2004**, *104*, 293.
(2) Huang, F.; Deng, Y.; Chen, Y.; Cai, X.; Peng, M.; Jia, Z.; Ren, P.; Xiao, D.; Wen, X.; Wang, N.; et al. *J. Am. Chem. Soc.* **2018**, *140*, 13142−13146.
(3) Kaizuka, K.; Miyamura, H.; Kobayashi, S. *J. Am. Chem. Soc.* **2010**, *132*, 15096−15098.
(4) Zhai, Q.; Xing, H.; Zhang, X.; Li, J.; Wang, E. K. *Anal. Chem.* **2017**, *89*, 7788−7794.
(5) Zhou, Q.; Lin, Y.; Xu, M.; Gao, Z.; Yang, H.; Tang, D. P. *Anal. Chem.* **2016**, *88*, 8886−8892.
(6) Pinheiro, A. V.; Han, D.; Shih, W. M.; Yan, H. *Nat. Nanotechnol.* **2011**, *6*, 763.
(7) Sadowski, J. P.; Calvert, C. R.; Zhang, D. Y.; Pierce, N. A.; Yin, P. *ACS Nano* **2014**, *8*, 3251−3259.
(8) Li, N.; Wang, M.; Gao, X.; Yu, Z.; Pan, W.; Wang, H.; Tang, B. *Anal. Chem.* **2017**, *89*, 6670−6677.
(9) Wang, S.; Xia, M.; Liu, J.; Zhang, S.; Zhang, X. *ACS Sens.* **2017**, *2*, 735−739.
(10) Li, J.; Pei, H.; Zhu, B.; Liang, L.; Wei, M.; He, Y.; Chen, N.; Li, D.; Huang, Q.; Fan, C. H. *ACS Nano* **2011**, *5*, 8783−8789.
(11) Mathur, D.; Samanta, A.; Oh, E.; Díaz, S. A.; Susumu, K.; Ancona, M. G.; Medintz, I. L. *Chem. Mater.* **2017**, *29*, 5762−5766.
(12) Lee, M. H.; Yang, Z.; Lim, C. W.; Lee, Y. H.; Dongbang, S.; Kang, C.; Kim, J. S. *Chem. Rev.* **2013**, *113*, 5071−5109.
(13) Zhou, Z.; Song, J.; Nie, L.; Chen, X. *Chem. Soc. Rev.* **2016**, *45*, 6597−6626.
(14) Estrela, J. M.; Ortega, A.; Obrador, E. *Crit. Rev. Clin. Lab. Sci.* **2006**, *43*, 143−181.
(15) Burridge, P. W.; Li, Y. F.; Matsa, E.; Wu, H.; Ong, S. G.; Sharma, A.; Holmström, A.; Chang, A. C.; Coronado, M. J.; Ebert, A. D.; et al. *Nat. Med.* **2016**, *22*, 547−556.
(16) Li, F.; Lin, Y.; Lau, A.; Tang, Y.; Chen, J.; Le, X. C. *Anal. Chem.* **2018**, *90*, 8651−8657.
(17) Sheng, L.; Lu, Y.; Deng, S.; Liao, X.; Zhang, K.; Ding, T.; Gao, H.; Liu, D.; Deng, R.; Li, J. *Chem. Commun.* **2019**, *55*, 10096−10099.
(18) Lu, L. M.; Zhang, X. B.; Kong, R. M.; Yang, B.; Tan, W. H. *J. Am. Chem. Soc.* **2011**, *133*, 11686−11691.
(19) Gorren, A. C.; Schrammel, A.; Schmidt, K.; Mayer, B. *Arch. Biochem. Biophys.* **1996**, *330*, 219−228.
(20) Viguier, R. F.; Hulme, A. N. *J. Am. Chem. Soc.* **2006**, *128*, 11370−11371.
(21) Hikosou, D.; Saita, S.; Miyata, S.; Miyaji, H.; Furuike, T.; Tamura, H.; Kawasaki, H. *J. Phys. Chem. C* **2018**, *122*, 12494−12501.
(22) Ma, M. N.; Zhuo, Y.; Yuan, R.; Chai, Y. Q. *Anal. Chem.* **2015**, *87*, 11389−11397.
(23) Shang, L.; Azadfar, N.; Stockmar, F.; Send, W.; Trouillet, V.; Bruns, M.; Gerthsen, D.; Nienhaus, G. U. *Small* **2011**, *7*, 2614−2620.
(24) Dou, X.; Yuan, X.; Yu, Y.; Luo, Z.; Yao, Q.; Leong, D. T.; Xie, J. *Nanoscale* **2014**, *6*, 157−161.
(25) He, Y.; Ye, T.; Su, M.; Zhang, C.; Ribbe, A. E.; Jiang, W.; Mao, C. *Nature* **2008**, *452*, 198.
(26) Hesari, M.; Workentin, M. S.; Ding, Z. *ACS Nano* **2014**, *8*, 8543−8553.
(27) Zhao, M.; Chen, A.; Huang, D.; Zhuo, Y.; Chai, Y.; Yuan, R. *Anal. Chem.* **2016**, *88*, 11527−11532.
(28) Xiao, Y.; Zhou, J.; Chen, M.; Wen, W.; Zhang, X.; Wang, S. *Chem. Commun.* **2018**, *54*, 10467−10470.
(29) Jung, Y. L.; Park, J. H.; Kim, M. I.; Park, H. G. *Nanotechnology* **2016**, *27*, 055501.
(30) Olmos Moya, P. M.; Martínez Alfaro, M.; Kazemi, R.; Alpuche-Avilés, M. A.; Griveau, S.; Bedioui, F.; Gutiérrez Granados, S. *Anal. Chem.* **2017**, *89*, 10726−10733.
(31) Wang, Y.; Lu, J.; Tang, L.; Chang, H.; Li, J. *Anal. Chem.* **2009**, *81*, 9710−9715.